Effect of inorganic salts on N'containing organic compounds formed by heterogeneous reaction of NO2 with oleic acid

The Effect of Inorganic Salts on N-Containing Organic Compounds Formed by Heterogeneous Reaction of NO_2 with Oleic Acid

Huifan Deng[1,4], Jiangping Liu[1,4], Yiqun Wang[1,4], Wei Song [1,2,3], Xinming Wang[1,2,3], Xue Li[5*], Davide Vione[6], Sasho Gligorovski[1,2,3*]

[1]State Key Laboratory of Organic Geochemistry and Guangdong Provincial Key Laboratory of Environmental Protection and Resources Utilization, Guangzhou Institute of Geochemistry, Chinese Academy of Sciences, Guangzhou 510 640, China

[2]Guangdong-Hong Kong-Macao Joint Laboratory for Environmental Pollution and Control, Guangzhou Institute of Geochemistry, Chinese Academy of Science, Guangzhou 510640, China

[3]Chinese Academy of Science, Center for Excellence in Deep Earth Science, Guangzhou, 510640

[4]University of Chinese Academy of Sciences, Beijing, China

[5]Institute of Mass Spectrometry and Atmospheric Environment, Jinan University, Guangzhou 510632, China

[6]Dipartimento di Chimica, Università degli Studi di Torino, Via Pietro Giuria 5, 10125 Torino, Italy

*Corresponding authors:
Sasho Gligorovski
gligorovski@gig-ac.cn
Xue Li
tamylee@jnu.edu.cn

Keywords: Oleic Acid, Heterogeneous Reactions, Nitrogen Oxides, Nitrous Acid, Nitroaromatic Compounds, Urban Air Pollution, Indoor Air.

Abstract

Fatty acids are ubiquitous constituents of grime on urban and indoor surfaces, and they represent important surfactants on organic aerosol particles in the atmosphere. Here, we assess the heterogeneous processing of NO_2 on films consisting of pure oleic acid (OA), or a mixture of OA and representative salts for urban grime and aerosol particles, namely Na_2SO_4 and $NaNO_3$. The uptake coefficients of NO_2 on OA under light irradiation ($300nm < \lambda < 400nm$) decreased with increasing relative humidity RH, from $(1.4 \pm 0.1) \times 10^{-6}$ at 0 % RH to $(7.1 \pm 1.6) \times 10^{-7}$ at 90 % RH. The uptake process of NO_2 on OA gives HONO as reaction product, and the highest HONO production was observed upon heterogeneous reaction of NO_2 with OA in the presence of nitrate (NO_3^-) ions. The formation of gaseous nitroaromatic compounds was also enhanced in the presence of NO_3^- ions upon light-induced heterogeneous processing of NO_2 with OA. These results suggest that inorganic salts can affect the heterogeneous conversion of gaseous NO_2 on fatty acids, and enhance the formation of HONO and other N-containing organic compounds in the atmosphere.

Introduction

Atmospheric aerosol particles are loaded with organic and inorganic compounds.[1] Organic compounds can affect the optical properties and hygroscopic growth of aerosol particles, and they can influence the heterogeneous reactions between oxidant species and inorganic constituents.[2] Among the organic compounds, fatty acids are emitted in the air by coal burning[3] and cooking[4-6]. They represent an important fraction of the organic compounds in aerosol and, because of amphiphilic properties and poor solubility in the aqueous phase, they act as surfactants and tend to form a coating over the particle core.[7] The surface of aerosols that mainly contain sulfate (SO_4^{2-}) and nitrate (NO_3^-) can for instance be enriched with unsaturated fatty acids.[8] Oleic acid, (OA, $C_{18}H_{34}O_2$) or 9-octadecenoic acid is an unsaturated fatty acid that is routinely detected in atmospheric aerosol particles and can be used as a marker compound for cooking.[9,10] Recently, real-time measurements in indoor environments detected over 600 compounds among primary cooking emissions and secondary products formed upon reactions with hydroxyl radicals (OH).[11] Among all the detected compounds, 183 features were identified as unsaturated or saturated fatty acids, and OA was the most abundant unsaturated fatty acid.[11] The reaction of ozone with OA as a proxy for unsaturated fatty acids has been extensively studied in the past, to better understand the oxidation processes affecting aerosol particles.[12-20] Studies have also been carried out, concerning the oxidative processing of OA by other relevant atmospheric oxidants (radicals) such as hydroxyl (OH),[21] nitrate (NO_3),[14] and chlorine (Cl).[22]

The organic compounds adsorbed on urban grime can be oxidized by atmospheric oxidants and affect urban air quality.[23,24] In addition to the fatty acids and polycyclic aromatic hydrocarbons (PAHs), urban grime contains salts such as nitrate and sulfate that are major species in grime and are very stable within the organic film.[25,26] The average concentrations of SO_4^{2-} and NO_3^- were reported as 7.6 μg cm^{-2} and 1.5 μg cm^{-2}, respectively.[26]

Nitrate photolysis on grime, on airborne particles and other environmental surfaces has been suggested to produce reactive nitrogen species such as NO, NO_2, and HONO.[23,27,28] It has also been suggested that light-induced heterogeneous reactions of NO_2 on simulated urban grime represent a source of HONO in the urban atmosphere.[23,29-32] Recently, it has been shown that light-enhanced NO_2 uptake on real urban grime gives high HONO yields, which are largely dependent on the relative humidity (RH%).[24] Indeed, light intensity, RH, temperature (T), and NO_2 concentrations all impact the NO_2 uptake and the HONO formation yields on various environmental surfaces.[24,33-41]

To date, no study has investigated the kinetics or reported the formation of HONO upon reaction of NO_2 with OA. In this study, for the first time to our best knowledge, we investigate the influence of RH% and light intensity on the heterogeneous reaction of NO_2 with an organic film consisting of: *(i)* oleic acid (OA); *(ii)* a mixture of OA and sodium sulfate (Na_2SO_4), and *(iii)* a mixture of OA and sodium nitrate ($NaNO_3$). The study was carried out in a well-established flow tube reactor, simultaneously coupled to a NO_x analyser to follow the NO_2 decay and to a membrane inlet single photon ionization time of flight mass spectrometer (MI-SPI-TOFMS) for online measurements of the secondarily

formed volatile organic compounds (VOCs). The HONO yields were detected indirectly with a coated Na_2CO_3 denuder.

We show that the NO_2 uptake coefficients on solid OA films decrease as a function of RH. The presence of Na_2SO_4 and $NaNO_3$ suppresses NO_2 reactivity, but yet the increase of RH leads to an increase in the NO_2 uptakes on OA/Na_2SO_4 and OA/$NaNO_3$ mixtures. The reaction pathway of HONO and nitroaromatic compounds formation are discussed.

Materials and methods

Film preparation

Rectangular glass plates (45 cm length × 1.5 cm width) were coated with films containing either OA, a mixture of OA and Na_2SO_4, or OA and $NaNO_3$. To do so, a fresh solution was prepared by dissolving 0.05 mg of OA, or OA mixed with the inorganic salts (either Na_2SO_4 or $NaNO_3$, 1:1 m/w) (Macklin, China) into 10 mL of dichloromethane (DCM) (Macklin, China), after which the liquid system was sonicated for about 10 min. It was then uniformly injected with a syringe on the glass plate, and let dry overnight.

The flow tube reactor

The flow tube reactor used to assess the heterogeneous reactions of NO_2 with the coated glass plates has been previously detailed,[24,42,43] and here only brief description is given. The glass plate coated with OA, OA/Na_2SO_4 or OA/$NaNO_3$ was inserted inside the flow tube reactor and exposed to NO_2, in the dark or under light irradiation.

Briefly, a NO_2 flow of 10 mL min^{-1} (0–100 mL min^{-1} HORIBA METRON mass flow controller; accuracy, ±1%) was mixed with 200 mL min^{-1} synthetic air flow (0-1000 mL min^{-1} HORIBA METRON mass flow controller; accuracy, ±1%). A sheath flow (N_2) of 1000 mL min^{-1} (0-1000 mL min^{-1} HORIBA METRON mass flow controller; accuracy, ±1%) was fed to a bubbler before its introduction inside the reactor, to obtain the atmospherically relevant NO_2 mixing ratios in ppb levels (40 to 50 ppb). The gas-phase NO_2 was injected into the flow tube reactor with a movable glass injector.

All the experiments were carried out at ambient temperature, 296±1 K, and the relative humidity (RH) varied between 0% and 90%.

Ion Analysis

Water-soluble anions were determined by ion analysis. Briefly, each glass plate was extracted with 5 mL ultra-pure water (Sartorius 18 M-ohm, H2O-MM88 UV-T, Germany) by sonication in an ultrasonic bath for 2 minutes. The extracts were then filtered with 0.22 μm IC Millex-LG filters and stored in pre-cleaned HDPE bottles. The samples (1 mL aliquots) were then diluted 10 times with ultra-pure water, prior to analysis by ion chromatography (Metrohm, 883 Basic IC plus) to detect the water-soluble anions of interest.

UV absorption spectra

The reacted glass plates were extracted with 10 mL DCM, and the UV spectra of OA, OA/Na_2SO_4, and OA/$NaNO_3$ in DCM were recorded with a UV-VIS double-beam spectrophotometer (Shanghai Drawell Scientific, China), using quartz cuvettes with 1 cm optical path length.

NO_x and HONO measurements

A saturated sodium carbonate (Na_2CO_3) solution was inserted into the denuder and let stand for more than half an hour, then the denuder was wrapped in tin foil and placed in an oven at about 106°C for drying. In this way, the denuder wall got coated with sodium carbonate crystals that are able to trap HONO (*vide infra*).

A chemiluminescence instrument (Eco Physics, model CLD 88p) connected with a photolytic (metal halide lamp) converter (Eco Physics, model PLC 860) was used to measure the NO_x signal at the end of the flow tube reactor. The detection limit of the NO_x analyzer was 10 ppt with a time resolution of 1s.[24]

The NO_x analyzer uses a chemiluminescence method to measure the NO_2 concentration, by converting NO_2 into NO with a molybdenum converter. With this method, one can directly measure NO without using the converter and NO_x = NO + NO_2 when the converter is operational, thus obtaining NO_2 as the difference between the two signals. HONO will also be converted to NO, thus it has the same analytical response as NO_2. The same NO_x analyzer was used to simultaneously measure NO_2 (directly) and HONO [33,34,37,44-46] (indirectly as described in SI).

Membrane inlet single photon ionization time of flight mass spectrometry (MI-SPI-TOFMS)

Membrane inlet single photon ionization time of flight mass spectrometry (MI-SPI-TOFMS) is a promising technique for the online monitoring of VOCs. A commercial MI-SPI-TOF-MS device (SPIMS 3000, Guangzhou Hexin Instrument Co., Ltd., China) was used in this study to monitor the gaseous product compounds formed upon heterogeneous reactions of NO_2 with surfaces

consisting of OA, OA/$NaNO_3$, or OA/Na_2SO_4. The details of this instrument are given elsewhere[47-49] and here only short description is given. Briefly, SPIMS 3000 consists of three parts: (1) a membrane inlet system, with a 0.002 inch thick permeable dimethylsiloxane (PDMS) membrane (Technical Production, Inc., U.S.A.) that concentrates the VOCs; (2) a single photon ionization (SPI) source, using a commercial deuterium lamp (Hamamatsu, Japan), and (3) a reflectron TOF-MS, which contains a double-pulsed acceleration region, a field-free drift tube, a reflector and an ion detector.[47] The raw data were analyzed by using commercial software (SPIMS 3000 V1.0.1.2.0, Guangzhou Hexin Instrument Co., Ltd., China), in which selected Gauss peaks above a preset threshold are smoothed with a given average number.[47-49]

The treatment of the uptake coefficients

The uptake coefficients of NO_2 (γ_{NO2}) on the coated glass plates were estimated as follows:

$$\gamma_{NO_2} = \frac{4 \times k_{1,NO_2}}{\overline{V_{NO_2}} \times A} \qquad \text{Eq-1}$$

where k_{1,NO_2} is the measured pseudo-first-order rate constant for the reaction between NO_2 and the coated glass surface, $\overline{V_{NO_2}}$ is the average molecular speed of gaseous NO_2, and A describes the geometry of the reactor as the ratio between the reactive surface (S) of the glass plate and the volume of the flow tube reactor (V).[24] The estimation of k_{1,NO_2} is described in the SI.

We performed test experiments in the empty reactor to check for photodissociation of NO_2 and formation of ozone. Indeed, NO_2 can be photolyzed with unit quantum yield in the wavelength region of 300-400 nm, where the lamps used in this study emit radiation (Atkinson, 2000, 2003). The photolysis rate of NO_2, ($J(NO_2)$), in a clean flow tube reactor under the experimental conditions applied in this study ranged from $1.4 \cdot 10^{-4}$ (s^{-1}) to $5.5 \cdot 10^{-4}$ (s^{-1}), which implies that

NO_2 degradation due to its photolysis was negligible (accounting for 0.1 to 0.6 % of the total NO_2). In addition, control experiments confirmed that there was no ozone production at the exit of the reactor, by coupling an ozone analyzer with the flow tube reactor.

Results and Discussion

The effect of RH

The uptake coefficients of NO_2 on oleic acid were investigated as a function of different RH values at 296 K (Figure 1). The NO_2 uptakes decreased linearly with increasing RH, from $(1.4 \pm 0.1) \times 10^{-6}$ at 0 % RH to $(7.1 \pm 1.6) \times 10^{-7}$ at 90 % RH, under light irradiation (15.5 W m^{-2}, 5.3×10^{13} photons cm^{-2} s^{-1}; 300nm < λ < 400nm).

The NO_2 uptake on OA at 0 % RH was slightly higher than the reactive uptake reported for NO_2 on real urban grime, $\gamma(NO_2) = (1.1 \pm 0.2) \times 10^{-6}$ at 0 % RH.[24] Although the NO_2 uptakes decreased with RH, the value $\gamma(NO_2) = (1.2 \pm 0.1) \times 10^{-6}$ observed at 30 % RH was still about 2 times higher than the reactive uptakes reported for NO_2 on simulated urban grime, made up of fluoranthene/KNO_3 ($\gamma(NO_2) = 6.6 \times 10^{-7}$ at 35 % RH) and phenantrene/KNO_3 ($\gamma(NO_2) = 7.8 \times 10^{-7}$ at 35 % RH).[33]

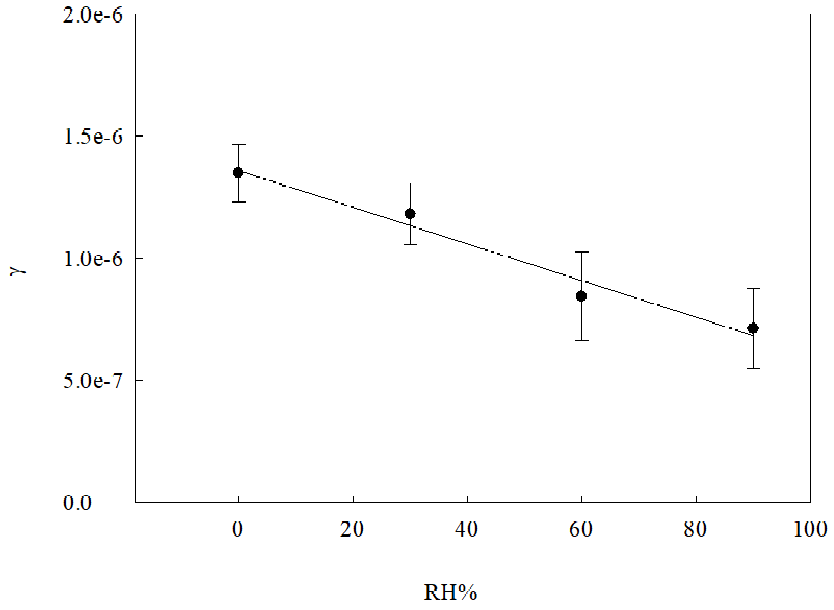

Figure 1: NO_2 uptake coefficients on ●) OA as a function of RH, at a NO_2 mixing ratio of 40 ppb and under light irradiation (15.5 W m^{-2}, 5.3×10^{13} photons cm^{-2} s^{-1}; 300nm < λ < 400nm) at 296 K. The error bars are derived from the uncertainties associated to the estimation of the uptake coefficients.

The decrease of the NO_2 uptakes with increasing RH observed here is completely opposite to the dependence of the NO_2 uptakes on fluorene (FL) and FL/Na_2SO_4, where a non-linear increase of NO_2 uptakes was observed with increasing RH.[43]

Considering that OA is poorly soluble in water, when RH increases, the formation of a water layer may occur above OA that reduces the accessibility of NO_2 to the adsorption sites on OA. Considering that the melting point of OA is 288 K, the OA film is expected to be liquid at 296 K. Therefore, most likely, reversible adsorption of water occurs on liquid OA and leads to displacement or competition for adsorption with NO_2.

If this is the case, at 90 % RH the measured uptake coefficient of NO_2 on OA should correspond to the uptake coefficient of NO_2 on a water layer. To verify this hypothesis, we measured the NO_2 uptake coefficients on a clean glass plate at 90 % RH in the absence of any organics. The uptake coefficient obtained in these conditions was $(7.6 \pm 0.5) \times 10^{-7}$, which is similar to the NO_2 uptake of $(7.1 \pm 1.6) \times 10^{-7}$ measured on the OA film at 90 % RH, and implies that OA is not accessible for NO_2 at 90% RH.

The addition to OA of Na_2SO_4 and $NaNO_3$ inhibited substantially the uptake of NO_2 at 0 % RH: it passed from $\gamma(NO_2) = (1.4 \pm 0.1) \times 10^{-6}$ without salts to $\gamma(NO_2) = (7.7 \pm 1.7) \times 10^{-7}$ with Na_2SO_4, and $\gamma(NO_2) = (4.7 \pm 2.4) \times 10^{-7}$ with $NaNO_3$. Conversely, the uptake coefficient of NO_2 on a mixture OA/Na_2SO_4 was $(1.5 \pm 0.5) \times 10^{-6}$ at 90 % RH, which is similar to $\gamma(NO_2) = (1.4 \pm 0.1) \times 10^{-6}$ on OA at 0 % RH. Indeed, increasing RH led to an increase of the NO_2 uptakes on both films, OA/Na_2SO_4 and OA/$NaNO_3$ (Figure 2).

The obtained NO_2 uptake coefficients on OA/$NaNO_3$ in the dark (Figure 2) are very similar to those observed under irradiation, which could be ascribed to the light-absorbing properties of OA/$NaNO_3$ and to the spectral irradiance emitted by the lamps. Namely, Figure S1 shows that the absorption spectrum of OA/$NaNO_3$ only slightly overlaps with the emission spectrum of the lamps in the near-UV region ($300 \text{ nm} < \lambda < 400 \text{ nm}$).

Similarly, a linear increase with RH of the uptake coefficients of ozone on a liquid film consisting of acetosyringone and Na_2SO_4 has been reported previously.[50]

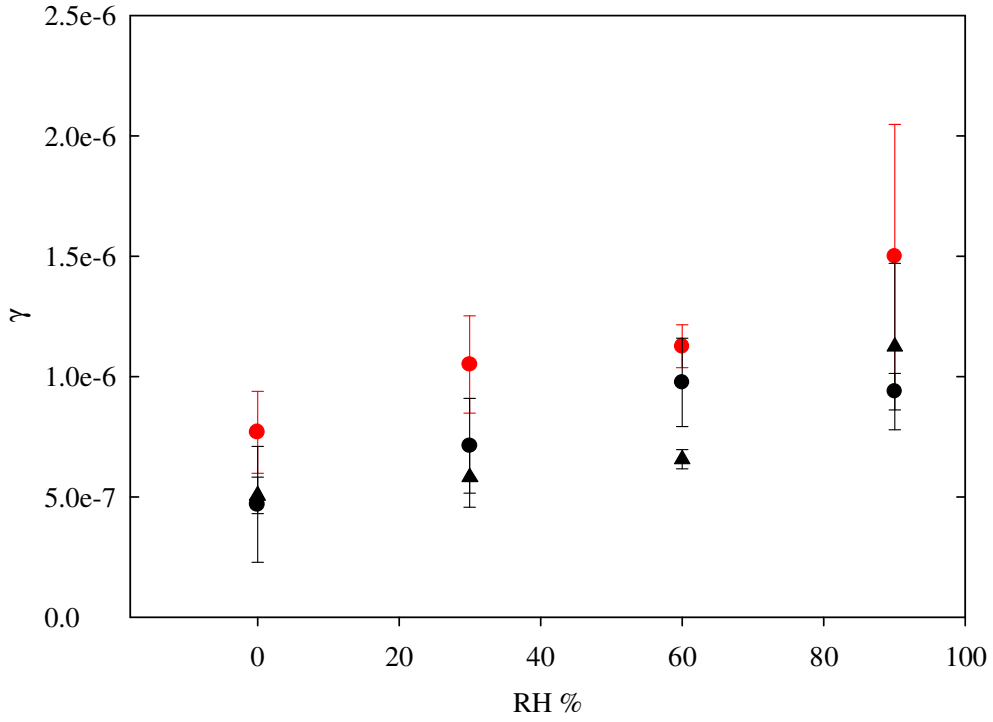

Figure 2: NO_2 uptake coefficients on ●) $OA/NaNO_3$ and ●) OA/Na_2SO_4, as a function of RH at NO_2 mixing ratio of 40 ppb, and light irradiation (15.5 W m^{-2}, 5.3 × 10^{13} photons cm^{-2} s^{-1}; 300nm < λ < 400nm) at 296 K. NO_2 uptake coefficients on ▲) $OA/NaNO_3$ under dark conditions. The error bars are derived from the uncertainties associated to the estimation of the uptake coefficients.

In the presence of NO_3^- ions, at higher RH, the liquid film becomes deliquesced, which implies that OA can reach the surface of the aqueous solution. The film must then be considered as a concentrated salt solution covered by a monolayer of OA, with a remaining liquid OA phase attached somewhere. This remaining liquid depends on how much OA is available and on the estimated density of the OA monolayer. The increasing solution volume could possibly induce an increasing surface area of the solution, thereby allowing for more OA being exposed to NO_2. However, Figure S3 shows a decrease of TIC when RH reaches 90 %, upon heterogeneous reaction of NO_2 with $OA/NaNO_3$ in the dark. It is thus possible that the surface concentration of OA decreases when it is "diluted" with $NaNO_3$, and the increase in both NO_2 uptakes and HONO

formation with increasing RH can be ascribed solely to the effect of NO_3^- on the heterogeneous reaction between NO_2 and OA (see section "Reaction Mechanism").

Influence of light intensity

The effect of the light intensity on the NO_2 uptake coefficients measured on OA, OA/Na_2SO_4, and OA/$NaNO_3$ was also evaluated by changing the number of lamps that irradiated the coated glass plates in the flow tube reactor. The uptake coefficients of NO_2 on OA were almost independent of the light intensity, as they ranged between $(5.6 \pm 0.9) \times 10^{-7}$ at 4.1 W m^{-2} and $(6.9 \pm 0.6) \times 10^{-7}$ at 15.5 W m^{-2} (Figure 3).

When OA was mixed with Na_2SO_4, the NO_2 uptakes slightly increased from $(9.0 \pm 3.8) \times 10^{-7}$ at 4.1 W m^{-2} to $(1.4 \pm 0.2) \times 10^{-6}$ at 15.5 W m^{-2}. In contrast, in the case of OA + $NaNO_3$ simultaneously exposed to NO_2 and light, there was a significant increase in the NO_2 uptakes by a factor of about 2 (Figure 3), from $(1.2 \pm 0.5) \times 10^{-6}$ at 4.1 W m^{-2} to $(2.7 \pm 0.3) \times 10^{-6}$ at 15.5 W m^{-2}. This latter finding could be ascribed to the increased overlap of the emission spectrum of 3 and 4 UV lamps with the absorption spectrum of OA/$NaNO_3$ (Figure S1).

From the regression line of the plot of γ versus light intensity, Eq. 2 is obtained that can be used to predict the uptake coefficient of NO_2 on OA/$NaNO_3$ under realistic light intensity, which is here expressed in W m^{-2} in the near-UV region of the solar spectrum (300 nm $<\lambda<$ 400 nm) at different solar zenith angles (SZA):

$\gamma = (6.3 \pm 2.2) \times 10^{-7} + (1.3 \pm 0.2) \times 10^{-7} \cdot$ light intensity / W m^{-2} Eq-2

$r^2 = 0.99$

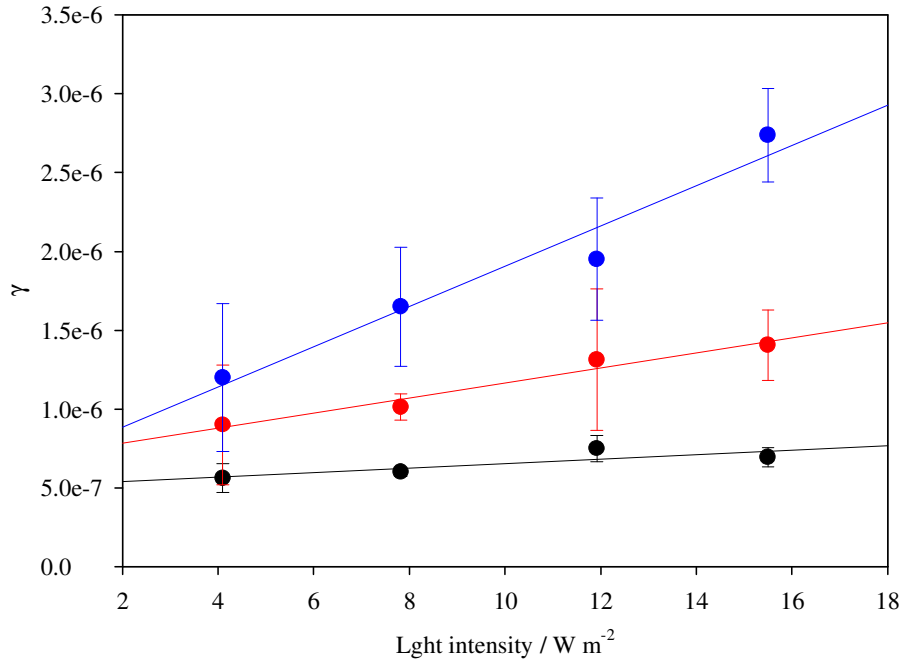

Figure 3: NO_2 uptake coefficients on ●) OA; ●) OA/Na_2SO_4, ●) OA/$NaNO_3$ as a function of the photon flux, at a NO_2 mixing ratio of 40 ppb and with 40 % RH at 296K. The error bars are derived from the uncertainties associated to the estimation of the uptake coefficients. The black, red, and blue lines represent the regression lines for the dependence of the NO_2 uptakes on OA, OA/Na_2SO_4, and OA/$NaNO_3$, respectively.

It is interesting to compare, with previous studies, the extrapolated NO_2 uptake coefficient on a film consisting of OA/$NaNO_3$ adsorbed on urban grime, at a UV radiation intensity of 46 W m^{-2} for the wavelength range between 300 and 400 nm (which corresponds to a solar zenith angle of 48° as given by National Renewable Energy Laboratory (NREL)[52]), which would be $\gamma = 6.6 \times 10^{-6}$. This value is of the same order of magnitude as the uptake coefficient of NO_2 on pyrene,[29] $\gamma = 8.8 \times 10^{-6}$ at 50 ppb of NO_2, and it is about 4 times higher than the uptake coefficient of NO_2 on simulated soot made up of gentisic acid ($\gamma = 1.6 \times 10^{-6}$, obtained at a NO_2 mixing ratio of 20 ppb and 20 % RH, under UV-VIS light irradiation at 40° solar zenith angle).[32] The uptake of NO_2 (20 ppb) on fluoranthene, $\gamma = 1 \times 10^{-6}$, [33] was about 7 times lower than the uptake of NO_2

on $OA/NaNO_3$ as determined in this study ($\gamma = 6.6 \times 10^{-6}$). Moreover, our latter value (6.6×10^{-6}) is 1.5 times lower than the NO_2 uptake on a solid film of fluorene, obtained at a NO_2 mixing ratio of 40 ppb and 60 % RH, under light intensity of 46 W m^{-2} for λ = 300-400nm.[43] Our value is also 1.5 times lower than the uptake coefficient of NO_2 measured on a simulated soil surface consisting of humic acid ($\gamma = 1 \times 10^{-5}$) under an irradiation intensity of 400 W m^{-2}, in the visible range of wavelengths (λ = 400-700nm) at 48° solar zenith angle, with NO_2 mixing ratio of 30 ppb, T= 298 K, and 30% RH.[34]

The extrapolated NO_2 uptake coefficient (Eq-3) on a OA/Na_2SO_4 film under the same irradiation conditions would be $\gamma = 2.9 \times 10^{-6}$, which is about 2 times lower than the value of γ on $OA/NaNO_3$, but still ca. 3 times higher than the NO_2 uptakes on gentisic acid, $\gamma = 1.6 \times 10^{-6}$, and on fluoranthene, $\gamma = 1 \times 10^{-6}$.[32,33] With OA/Na_2SO_4 one gets the following equation:

$$\gamma = (6.9 \pm 0.7) \times 10^{-7} + (4.8 \pm 0.6) \times 10^{-8} \cdot \text{light intensity / W m}^{-2} \qquad \text{Eq-3}$$

$r^2 = 0.96$

Finally, the extrapolated NO_2 uptake coefficient on a film containing only pure OA (Eq-4) under the same irradiation conditions would be 1.2×10^{-6}, which falls in the range of the NO_2 uptakes on gentisic acid, $\gamma = 1.6 \times 10^{-6}$, [32] and fluoranthene, $\gamma = 1 \times 10^{-6}$. [33]

$$\gamma = (5.1 \pm 0.7) \times 10^{-7} + (1.4 \pm 0.7) \times 10^{-8} \cdot \text{light intensity / W m}^{-2} \qquad \text{Eq-4}$$

$r^2 = 0.7$

Considering that in the UV range of wavelengths, the light flux in the indoor environment is 9 W m^{-2}, [53] the interpolated NO_2 uptake coefficients would be 1.8×10^{-6}, 1.1×10^{-6}, and 6.4×10^{-7} in the cases of $OA/NaNO_3$, OA/Na_2SO_4 and OA, respectively. Although these uptakes are relatively low when compared to the corresponding values obtained for urban grime under a UV light intensity of 46 W m^{-2} (see above), the observed HONO yields generated by NO_2 conversion on

$OA/NaNO_3$, OA/Na_2SO_4 and OA (*vide infra*) can have health implications for the inhabitants that inhale HONO.[54,55] Moreover, HONO photolysis and the associated production of hydroxyl radicals (OH) may play a key role in the formation of toxic secondary compounds in urban and indoor air.[11,48,56-59]

Comparison between spectral irradiance and UV absorption spectra

To understand the dependence of the uptake coefficients on the light intensity (Figure 3), we measured the spectral irradiance of the four UV lamps used to irradiate the glass plates in our flow tube reactor, and compared it with the UV-VIS absorption spectra of the coated (OA, OA/Na_2SO_4, $OA/NaNO_3$) glass plates (Figure S1).

Figure S1 shows only a slight overlap of spectral irradiance with UV absorption spectra, when one or two UV lamps were used. This is the most likely reason for the very similar values of the NO_2 uptake coefficients measured on $OA/NaNO_3$, in the dark and under irradiation with two lamps (Figure 2). By increasing the number of lamps one has stronger overlap between the film absorption spectra and the lamp spectral irradiance, which may explain the increase of the uptake coefficients with the light intensity shown in Figure 3, especially in case of $OA/NaNO_3$.

It is known that nitrates can absorb UVB as well as short-wavelength UVA radiation and produce HONO after the photodissociation process.[27,28] The photolysis rate constant of HNO_3 adsorbed on borosilicate glass (the same material as the glass plates used in this study) has been reported as 1.2×10^{-5} s^{-1} at 50% RH, which is two orders of magnitude higher compared to liquid-phase and gas-phase HNO_3 under comparable irradiation conditions.[27] Moreover, solid nitrate near the surface does not undergo the solvent-cage effect that is experienced in aqueous solutions, where photogenerated $OH + NO_2$ are initially surrounded by a cage of water molecules

that favour the recombination to $NO_3^- + H^+$ at the expense of diffusion of OH and NO_2 into the solution bulk. Indeed, the solvent-cage effect decreases the net rate of NO_3^-/HNO_3 photolysis in solution (*vide infra*).[60]

HONO and NO formation yields

When the NO_x analyzer was directly hyphenated to the flow tube reactor, a decrease of the NO_2 signal was observed due to the uptake of NO_2 by the OA film. When the Na_2CO_3 denuder was connected between the flow tube reactor and the NO_x analyzer, an additional decrease of the NO_2 signal was observed that corresponds to the HONO trapped by the denuder. The HONO mixing ratio was obtained as the difference between the NO_2 signals without and with the Na_2CO_3 denuder.

The HONO and NO formation yields through light-induced heterogeneous conversion of NO_2 on films containing OA, OA/Na_2SO_4, and OA/$NaNO_3$ were calculated as the ratios $\Delta HONO/\Delta NO_2$ and $\Delta NO/\Delta NO_2$, respectively (Table 1). Table 1 shows that the HONO and NO yields only slightly varied with the RH. The most efficient conversion of NO_2 to HONO was observed with OA/$NaNO_3$ in the dark, with HONO yields ranging from 26 % at 30 % RH, to 62 % in the absence of RH. Under light irradiation the most efficient HONO formation was also observed with OA/$NaNO_3$, with HONO yields ranging from 30 % at 30 % RH to 49 % at 60 % RH. This finding suggests that nitrate promotes the conversion process of NO_2 to HONO on the fatty acid surface (Table 1).

Table 1: The formation yields of HONO and NO in dark and under light irradiation (15.5 W m^{-2}) with different RH values, at 40 ppb of NO_2 and 293 K.

	Oleic Acid				Oleic Acid + Na_2SO_4				Oleic Acid + $NaNO_3$			
	dark		light		dark		light		dark		light	
RH%	HONO yield	NO yield	HONO yield	NO yield	HONO yield	NO yield	HONO yield	NO yield	HONO yield	NO yield	HONO yield	NO yield
0%	11.8%	4.8%	17.2%	9.2%	18.5%	7.7%	28.7%	8.4%	62.2%	15.2%	44.5%	10.6%
30%	15.9%	0.5%	31.9%	22.5%	15.6%	7.7%	19.7%	6.4%	25.5%	3.8%	30.4%	10.4%
60%	25.9%	5.1%	28.1%	9.2%	13.9%	6.0%	25.7%	4.0%	47.4%	9.5%	49.0%	5.6%
90%	26.0%	3.3%	30.8%	8.8%	30.6%	2.0%	27.8%	4.1%	36.5%	4.5%	40.3%	24.6%

Table S7 shows the effect of nitrate ions on HONO formation, in the dark and under light irradiation. It can be seen from Table S7 that the quantity of HONO (ΔHONO) formed upon reaction of NO_2 with OA/$NaNO_3$ under light irradiation is higher than that in dark, especially at high RH. At the same time, however, NO_2 uptake increased as well and the overall HONO yield was almost unchanged. It can also be seen that the formed amount of HONO, during the light-induced reaction of NO_2 with OA/$NaNO_3$, increased with increasing RH.

The ion chromatography analysis revealed that the quantity of NO_3^- at 60 % RH increased from 9 ppm before the reaction to, respectively, 24 and 22 ppm after 1 h of heterogeneous reaction of NO_2 with OA/$NaNO_3$, in the dark and under irradiation. These results suggest that at 60 % RH, 49 % of NO_2 was converted into gaseous HONO but the remaining ≈50 % was converted into nitric acid (HNO_3), which remained on the flow tube surface. The quantity of NO_2^- only slightly increased, from 0 ppm before the reaction to 0.067 and 0.008 ppm following the reaction of NO_2 with OA/$NaNO_3$, respectively in the dark and under irradiation. The amounts of NO_3^- and NO_2^-

ions also increased from 2 to 5 ppm, and from 0.017 to 0.027 ppm, respectively, after 1 h light-induced heterogeneous reaction of NO_2 with the OA film. Intriguingly, the quantity of NO_3^- and NO_2^- ions decreased from 0.003 to 0 ppm and from 0.04 to 0.006 ppm, respectively, after 1 h reaction of NO_2 with the film consisting of OA/Na_2SO_4 in the presence of light.

Gas-phase product compounds detected by MI-SPI-TOFMS analysis

The formation of gaseous compounds released upon heterogeneous reactions of NO_2 with OA, OA/$NaNO_3$, and OA/Na_2SO_4 at 30 % RH, in the dark and under irradiation was monitored on-line by MI-SPI-TOF-MS. The increase of RH to 90 % substantially reduced the total ion counts of the gas-phase compounds observed with NO_2 + OA (Figure S2), thereby confirming our hypothesis that at higher RH, OA is covered with a water layer that both inhibits the reaction and leads to lower NO_2 uptakes (Figure 1).

Figures S4-S6 report the signal intensities obtained from scans of mass to charge ratios (*m/z*) ranging between 50 and 250 amu, which are relevant to the observed gas-phase compounds formed upon reaction of NO_2 with OA, OA/$NaNO_3$, and OA/Na_2SO_4, in the dark and under irradiation with simulated sunlight, at 30 % RH. The main differences that can be observed are related to the presence of either $NaNO_3$ or Na_2SO_4 on the film consisting of OA. Namely, the presence of NO_3^- promotes the formation of N-containing organic compounds (see section "Reaction Mechanism"), and the presence of SO_4^{2-} increases substantially the number of the formed compounds. Tables S1–S3 summarize all the detected *m/z* values under different conditions, showing that the highest abundances occurred with OA/Na_2SO_4, both in the dark and under irradiation.

It can be seen from Figures S4-S6 that certain product peaks are separated by $\Delta m/z$ = 16, which corresponds to a multiple addition of O atoms that suggests the formation of carbonyl compounds and alcohols.[21] The oxidation of the saturated alkyl groups is in fact associated with an addition of 14 Da (carbonyl), and then by the 16 Da (hydroxyl) pattern (Figures S4-S6).[61]

Figure 4 shows typical profiles for the formation of gas-phase compounds upon reaction of NO_2 with OA and OA/$NaNO_3$, in the dark and under irradiation. The variation trend of five compounds (*m/z* 122, 142, 152, 156, and 166) formed upon heterogeneous reactions of NO_2 with OA is shown in Figure 4A. The profiles of those five products were very similar in the dark and in the presence of light. However, the presence of nitrate ions in the OA film suppressed the formation of VOCs in the dark (Table S2), but induced the formation of several new compounds (*m/z* 58, 81, 96, 110, 124, and 138) under irradiation (Figure 4B). MS data suggest that the latter compounds likely bear nitro groups. This finding indicates that the NO_3^- ions favor the formation of secondary nitro-organics as well as HONO, which would be released upon light-induced NO_2 reactions with OA. Figure S3 shows that the total ion current (TIC) at the different *m/z* values slightly decreased with increasing RH (from 30 to 90 % in the dark), but then increased again to the initial level upon light irradiation of OA/$NaNO_3$ at 90 % RH. When sulfate ions were present in the OA film, most of the gas-phase compounds were formed in the dark (Figure S4). Compared to the gas-phase compounds formed by reaction of NO_2 with OA and the OA/$NaNO_3$ surface, there were three distinct compounds (*m/z* 100, 188, 216) formed upon dark heterogeneous reaction of NO_2 with OA/Na_2SO_4 (Figure S7, Table S3). In addition there are some compounds, the intensities of which increase under light irradiation (*m/z* 57, 81, 124, 138) (Figure S7).

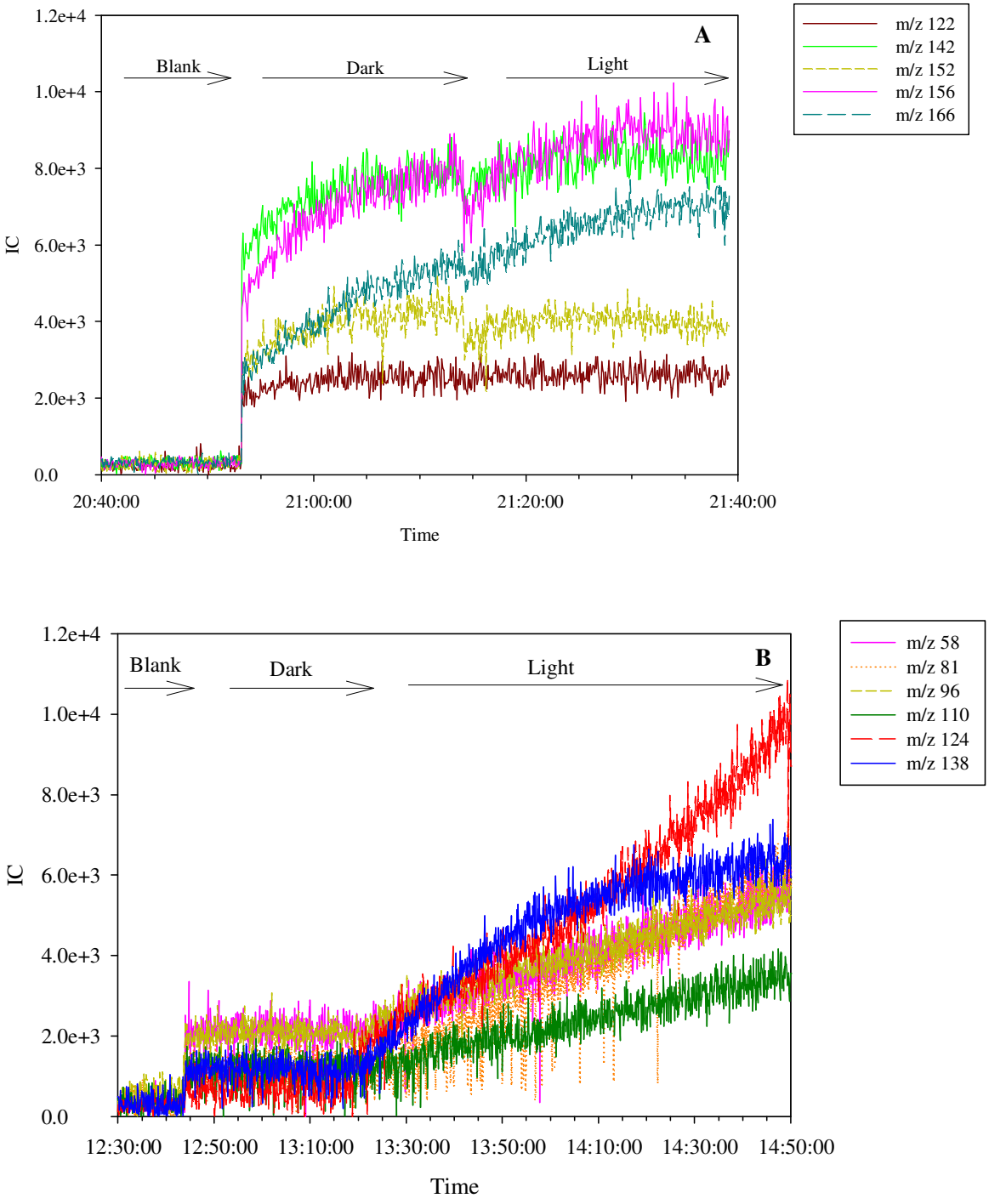

Figure 4: Typical profiles of gas-phase compounds formed upon heterogeneous reactions of NO_2 with A) OA and B) OA/$NaNO_3$.

Reaction mechanism

Unsaturated fatty acids such as OA contain double bonds, which are susceptible to NO_2 attack *via* either homolytic or heterolytic (ionic) reactions. A hydrogen (H) atom abstraction might also occur at the bis-allylic methylene center of OA, which leads to the formation of pentadienyl radicals.[62] The initial product compounds of H-abstraction by NO_2 from OA would be HONO and a resonance-stabilized allylic radical,[63] but H-abstraction is too slow to compete with NO_2 addition to the double bond.[64] Nevertheless, in the presence of oxygen, alkoxy radicals could arise from dissociation of peroxynitrates, as follows:[65]

$$RO\text{-}ONO_2 \rightarrow RO^{\bullet} + NO_3 \qquad \text{R-1}$$

The resulting alkoxy radicals could abstract H-atom from cyclohexene (*m/z* 82) to produce 2-cyclohexenol (*m/z* 98) (Tables-S1-S3).[64]

In the first step of oleic acid nitration, NO_2 adds to alkene double bonds via a fast and reversible process to initially form β-nitroalkyl radicals.[64] The reaction of the β-nitroalkyl radical with another NO_2 molecule might then proceed through H-abstraction, which would yield nitro-OA as well as HONO. This process, which can also take place in the dark, would produce HONO with 50% yield and might significantly contribute to HONO production, especially at low RH (Table 1). At the same time, non-volatile nitro-OA would remain attached to the film and would not contribute to the observed nitrated VOCs. In contrast, the formation of 50% HONO + 50% HNO_3 that was observed at 60% RH is consistent with the well-known hydrolysis pathway of NO_2 in the presence of a liquid phase:

$$2\ NO_2 \leftrightarrows N_2O_4 \xrightarrow{H_2O} HONO + H^+ + NO_3^- \qquad \text{R-2}$$

One of the gaseous products formed by NO_2 addition to the C=C bond is 1,2-dinitrocyclohexene (*m/z* 174)[64] which was also tentatively identified in this study (Tables S1, S3). A tentative

reaction pathway leading to the formation of this compound, assuming cyclohexene as the precursor, is provided in Scheme 1. Interestingly, the proposed addition-elimination pathway is exactly the opposite as the nitration of phenolic compounds by NO_2, which first proceeds via H-abstraction to produce HONO and a phenoxyl radical, followed by addition of another NO_2 to finally produce the nitrophenol.[66]

Scheme 1: Proposed reaction pathway for the formation of the tentatively detected compound 1,2-dinitrocyclohexene. Here we assume that cyclohexene derives from OA fragmentation.

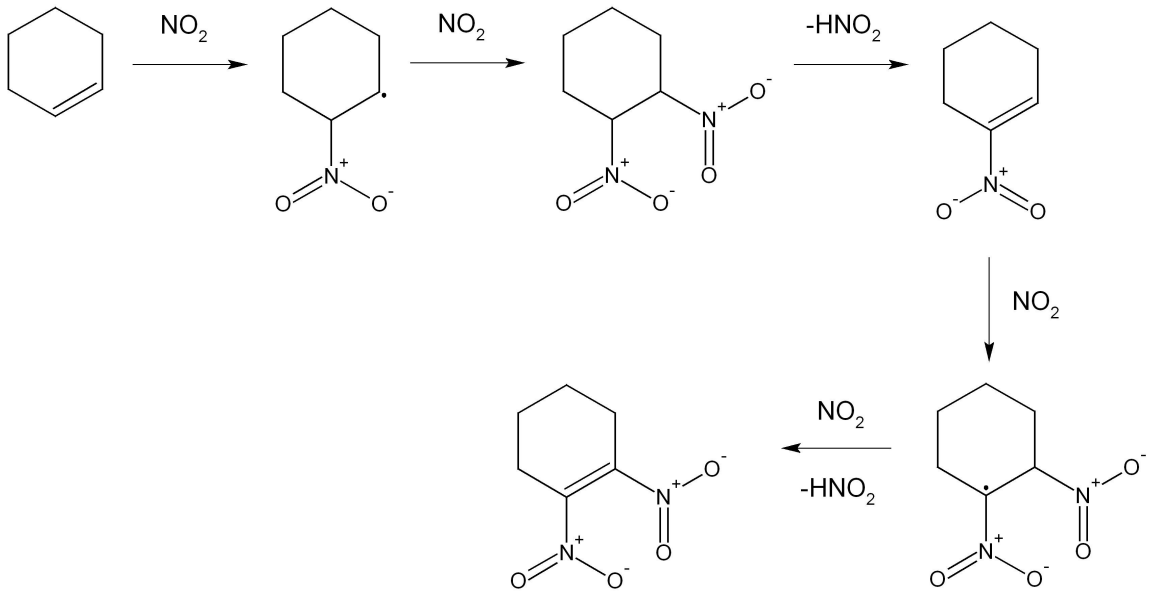

The relatively high HONO values formed at high RH in the presence of OA/$NaNO_3$ under irradiation (Table S7) could be accounted for by an additional process, yielding HONO from the

photochemistry of nitrate. Indeed, liquid-phase NO_3^- is a significant photochemical source of NO_2^-, and of gas-phase HONO as a consequence (see reaction sequence from R-3 to R-9).[67]

$$NO_3^- \xrightarrow{h\nu,\ H^+} [NO_2 + OH]_{cage} \quad \text{R-3}$$

$$[NO_2 + OH]_{cage} \rightarrow NO_3^- + H^+ \quad \text{R-4}$$

$$[NO_2 + OH]_{cage} \rightarrow NO_2 + OH \quad \text{R-5}$$

$$[NO_2 + OH]_{cage} + OA \rightarrow OA_{ox} + NO_2 \quad \text{R-6}$$

$$NO_3^- \xrightarrow{h\nu} NO_2^- + O \quad \text{R-7}$$

$$2\ NO_2 \leftrightarrows N_2O_4 \xrightarrow{H_2O} HONO + H^+ + NO_3^- \quad \text{R-8}$$

$$NO_2^- + H^+ \leftrightarrows HONO \quad \text{R-9}$$

$$NO_2^- \xrightarrow{h\nu, H^+} OH + NO \quad \text{R-10}$$

$$HONO \xrightarrow{h\nu} OH + NO \quad \text{R-11}$$

where OA_{ox} is a radical species arising from OH addition to OA. The occurrence of OA as OH scavenger could enhance the photoproduction of HONO, by inhibiting recombination between the geminate species produced by nitrate photolysis inside the solvent cage.[60] The photogeneration of OH by photolysis of nitrate and possibly of photogenerated NO_2^- and HONO (reactions R10, R11)[66] could give a significant contribution to the occurrence of oxidized/hydroxylated compounds.

At the same time, however, the hydroxyl radicals produced under irradiation could cause NO_2 oxidation and enhance its conversion. The increase in both HONO production and NO_2 processing might explain why the HONO yield changed very little with $NaNO_3$ in the dark or

under irradiation (Table 1), despite the increased production of HONO under irradiation (Table S7).

$NO_2 + OH \rightarrow NO_3^- + H^+$ R-12

Interestingly, the photolysis of the formed N-containing compounds such as 1,2-dinitrocyclohexene (Scheme 1) can be plausibly linked with HONO formation, as shown by R-13, which can be an additional photochemical source of HONO in urban environment.[68–70]

$R\text{-}NO_2 \xrightarrow{h\nu} R' + HONO$ R-13

Considering that fatty acids are ubiquitous surfactants in the atmospheric particles and on urban and indoor grime, the results from this study suggest that fatty acids play an important role in urban- and indoor air pollution through light-induced heterogeneous conversion of NO_2 into HONO. A comprehensive understanding of HONO formation processes is important with respect to the urban and indoor air chemistry, because HONO is the main source of OH radicals through its photolysis in the urban environment[57-59] and in sunlit regions of the indoor environment[56]. In particular, the formation of N-containing organic compounds through reaction of NO_2 with the OA can be of serious concern with respect to human health. The presence of NO_3^- ions during the heterogeneous NO_2 processing of OA favors the formation of nitroaromatic compounds, which are potential light-absorbing compounds that could affect both climate and air quality.

Associated content

Acknowledgment

This study was financially supported by the Chinese Academy of Science, International Cooperation Grant (N°: 132744KYSB20190007), National Natural Science Foundation of China (N°: 41773131, and N°: 41977187), State Key Laboratory of Organic Geochemistry, Guangzhou Institute of Geochemistry (SKLOG2020-5, and KTZ_17101) and Guangdong Foundation for Program of Science and Technology Research (N°: 2017B030314057).

Supporting Information

Additional 7 figures and 7 tables. The supporting information is available free of charge via the Internet on the ACS Publications website at http://pubs.acs.org.

Author information

Corresponding Authors

* Phone: +86 2085291497; Email: gligorovski@gig.ac.cn

* Phone: +86 2085221076; Email: tamylee@jnu.edu.cn

Notes

The authors declare no competing financial interest.

References：

1. Murphy, D. M.; Cziczo, D. J.; Froyd, K. D.; Hudson, P. K.; Matthew, B. M.; Middlebrook, A. M.; Peltier, R. E.; Sullivan, A.; Thomson D. S.; Weber, R. J. Single-particle mass spectrometry of tropospheric aerosol particles *J. Geophys. Res.: Atmos.*, 2006, *111(D23)*, D23S32.
2. Abbatt, J. P. D.; Lee A. K. Y.; Thornton, J. A. Quantifying trace gas uptake to tropospheric aerosol: recent advances and remaining challenges. *Chem. Soc. Rev.*, 2012, *41*, 6555-6581.
3. Oros, D. R.; Simoneit, B. R. T. Identification and emission rates of molecular tracers in coal smoke particulate matter. *Fuel*, 2000, *79(5)*, 515-536.
4. Schauer, J. J.; Rogge, W. F.; Hildemann, L. M.; Mazurek M. A.; Cass, G. R. Source apportionment of airborne particulate matter using organic compounds as tracers. *Atmos. Environ.*, 1996, *30(22)*, 3837-3855.
5. Schauer, J. J.; Kleeman, M. J.; Cass G. R.; Simoneit, B. R. T. Measurement of emissions from air pollution sources. 1. C1 through C29 organic compounds from meat charbroiling *Environ. Sci. Technol.*, 1999, *33*, 1566-1577.
6. Schauer, J. J.; Kleeman, M. J.; Cass G. R.; Simoneit, B. R. T. Measurement of emissions from air pollution sources. 4. C1 –C27 organic compounds from cooking with seed oils *Environ. Sci. Technol.*, 2002, *36*, 567-575.
7. Ren, L. J.; Fu, P. Q.; He, Y.; Hou, J. Z.; Chen, J.; Pavuluri, C. M.; Sun Y. L.; Wang, Z. F. Molecular distributions and compound-specific stable carbon isotopic compositions of lipids in wintertime aerosols from Beijing. *Sci Rep.*, 2016, *6*, 27481.
8. Tervahattu, H.; Juhanoja, J.; Vaida, V.; Tuck, A. F.; Niemi, J. V.; Kupiainen, K.; Kulmala M.; Vehkamaki, H. Fatty acids on continental sulfate aerosol particles. *J. Geophys. Res. Atmos.*, 2005, *110*, D06207.
9. Feng, J.; Hu, M.; Chan, C. K.; Lau, P. S.; Fang, M.; He, L.; Tang, X. A Comparative Study of the Organic Matter in PM2.5 from Three Chinese Megacities in three Different Climatic Zones. *Atmos. Environ.*, 2006, *40(21)*, 3983-3994.
10. Dreyfus M. A.; Johnston, M. V. Rapid Sampling of Individual Organic Aerosol Species in Ambient Air with the Photoionization Aerosol Mass Spectrometer. *Aerosol Sci. Technol.*, 2008, *42(1)*, 18-27.
11. Zeng, J. F.; Yu, Z. J.; Mekic, M.; Liu, J.; Li, S.; Loisel G.; Gao, W.; Gandolfo, A.; Zhou, Z.; Wang, X.; Herrmann, H.; Gligorovski, S.; Li, X. Evolution of indoor cooking emissions captured by using secondary electrospray ionization high resolution mass spectrometry, *Environ. Sci. Technol. Lett.*, 2020, *7, 2*, 76-81.
12. Moise, T.; Rudich, Y. Reactive Uptake of Ozone by Aerosol-Associated Unsaturated Fatty Acids: Kinetics, Mechanism, and Products *J. Phys. Chem. A.*, 2002, *106*, 6469-6476.
13. Knopf, D. A.; Anthony L. M.; Bertram, A. K. Reactive Uptake of O3 by Multicomponent and Multiphase Mixtures Containing Oleic Acid. *J. Phys. Chem. A.*, 2005, *109*, 5579-5589.
14. Hung, H.; Katrib Y.; Martin, S. T. Products and Mechanisms of the Reaction of Oleic Acid with Ozone and Nitrate Radical. *J. Phys. Chem. A.*, 2005, *109*, 4517-4530.

15. Robinson, A. L.; Subramanian, R.; Donahue, N. M.; Bernardo Bricker, A., and Rogge, W. F. Source Apportionment of Molecular Markers and Organic Aerosol. 3. Food Cooking Emissions. *Environ. Sci. Technol.*, 2006, *40(24*), 7820-7827.
16. McNeill, V. F.; Wolfe, G. M. and Thornton, J. A. The Oxidation of Oleate in Submicron Aqueous Salt Aerosols: Evidence of a Surface Process. *J. Phys. Chem. A*. 2007, *111*, 1073-1083.
17. Zahardis, J.; Petrucci, G. A. The oleic acid–ozone heterogeneous reaction system: products, kinetics, secondary chemistry, and atmospheric implications of a model system – a review. *Atmos. Chem. Phys.*, 2007, *7*, 1237–1274.
18. Vesna, O.; M, Sax; Kalberer, M.; Gaschen, A.; Ammann, M. Product study of oleic acid ozonolysis as function of humidity, *Atmos. Environ.*, 2009, *43*, 3662–3669.
19. Sage, A. M.; Weitkamp, E. A.; Robinson; A. L.; Donahue, N. M. Reactivity of oleic acid in organic particles: changes in oxidant uptake and reaction stoichiometry with particle oxidation, *Phys. Chem. Chem. Phys.*, 2009, *11*, 7951-7962.
20. Chu, Y. X.; Chan, C. K. Reactive Uptake of Dimethylamine by Ammonium Sulfate and Ammonium Sulfate–Sucrose Mixed Particles. *Aerosol Sci. Technol.*, 2017, *51*, 988–997.
21. Nah, T.; Kessler, S. H.; Daumit, K. E.; Kroll, J. H.; Leoneabe, S. R.; Wilson, K. R. OH-initiated oxidation of sub-micron unsaturated fatty acid particles，*Phys. Chem. Chem. Phys.*, 2013, *15*, 18649-18663.
22. Schwartz-Narbonne, H.; Wang, C.; Zhou, S. M.; Abbatt, J. P. D.; Faust, J. Heterogeneous Chlorination of Squalene and Oleic Acid. *Environ. Sci. Technol.*, 2019, *53(3)*, 1217-1224.
23. Baergen, A. M.; Donaldson, D. J. Photochemical renoxification of nitric acid on real urban grime. *Environ. Sci. Technol.,* 2013, *47*, 815-820.
24. Liu, J. P.; Li, S.; Mekic, M.; Jiang, H. Y.; Zhou, W. T.; Loisel, G.; Song, W.; Wang, X. M.; Gligorovski S. Photoenhanced uptake of NO_2 and HONO formation on real urban grime, *Environ. Sci. Technol. Lett.,* 2019, *6*, 413-417.
25. Baergen, A. M.; Styler, S. A.; Van Pinxteren, D.; Müller, K.; Herrmann, H.; Donaldson, D. J. Chemistry of urban grime: Inorganic ion composition of grime vs. particles in Leipzig. Germany. *Environ. Sci. Technol.*, 2015, *49 (21)*, 12688-12696.
26. Chabas, A.; Lombardo, T.; Cachier, H.; Pertuisot, M. H.; Oikonomou, K.; Falcone, R.; Verità, M.; Geotti-Bianchini, F. Behaviour of self-cleaning glass in urban atmosphere. *Build Environ.*, 2008, *43(12)*, 2124-2131.
27. Zhou, X.; Gao, H.; He, Y.; Huang, G.; Bertman, S. B.; Civerolo, K.; Schwab, J. Nitric Acid Photolysis on Surfaces in Low NOx Environments: Significant Atmospheric Implications. *Geophys. Res. Lett.*, 2003, *30*, 2217.
28. Zhou, X.; Zhang, N.; TerAvest, M.; Tang, D.; Hou, J.; Bertman, S.; Alaghmand, M.; Shepson, P. B.; Caroll, M. A.; Griffith, S.; Dusanter, S.; Stevens, P. S. Nitric Acid Photolysis on Forest Canopy Surface as a Source for Tropospheric Nitrous Acid. *Nat. Geosci.*, 2011, *4*, 440-443.
29. George, C.; Strekowski, R. S.; Kleffmann, J.; Stemmler, K.; Ammann, M. Photoenhanced uptake of gaseous NO_2 on solid organic compounds: a photochemical source of HONO? *Faraday Discuss.,* 2005, *130*, 195-210.
30. Brigante, M.; Cazoir, D.; D'Anna, B.; George, C.; Donaldson, D. J. Photoenhanced Uptake of NO_2 by Pyrene Solid Films. *J. Phys. Chem. A.*, 2008, *112*, 9503-9508.

31. Ammar, R.; Monge, M. E.; George, C.; D'Anna, B. Photoenhanced NO_2 Loss on Simulated Urban Grime. *ChemPhysChem.,* 2010, *11*, 3956-3961.
32. Sosedova, Y.; Rouvière, A.; Bartels-Rausch, T.; Ammann, M. UVA/Vis-induced nitrous acid formation on polyphenolic films exposed to gaseous NO_2. *Photochem. Photobiol. Sci.* 2011, *10*, 1680-1690.
33. Cazoir, D.; Brigante, M.; Ammar, R.; D'Anna, B.; George, C. Heterogeneous Photochemistry of Gaseous NO_2 on Solid Fluoranthene Films: A Source of Gaseous Nitrous Acid (HONO) in the Urban Environment. *J. Photochem. Photobiol. A Chem.*, 2014, *273*, 23-28.
34. Stemmler, K., Ammann, M., Donders, C., Kleffmann, J., George, C. Photosensitized reduction of nitrogen dioxide on humic acid as a source of nitrous acid., *Nature*, 2006, *440*, 195-198.
35. Stemmler, K.; Ndour, M.; Elshorbany, Y.; Kleffmann, J.; D'Anna, B.; George, C.; Bohn, B.; Ammann, M. Light induced conversion of nitrogen dioxide into nitrous acid on submicron humic acid aerosol. *Atmos. Chem. Phys.,* 2007, *7*, 4237-4248.
36. Ndour, M.; D'Anna, B.; George, C.; Ka, O.; Balkanski, Y.; Kleffmann, J.; Stemmler K.; Ammann, M. Photoenhanced uptake of NO_2 on mineral dust: Laboratory experiments and model simulations., *Geophys Res Lett.,* 2008, *35*, L05812.
37. Monge, M. E.; D'Anna, B.; George, C. Nitrogen dioxide removal and nitrous acid formation on titanium oxide surfaces-an air quality remediation process? *Phys. Chem. Chem. Phys.,* 2010, *12*, 8991-8998.
38. Monge, M. E.; D'Anna, B.; Mazri, L.; Giroir-Fendler, A.; Ammann, M.; Donaldson, D. J.; George, C. Light changes the atmospheric reactivity of soot. *Proc. Natl. Acad. Sci. U.S.A.*, 2010, *107(15)*, 6605-6609.
39. Gómez Alvarez, E.; Soergel, M.; Gligorovski, S.; Bassil, S.; Bartolomei, V.; Coulomb, B.; Zetzsch, C.; Wortham, H. Light-induced nitrous acid (HONO) production from NO_2 heterogeneous reactions on household chemicals. *Atmos. Environ.,* 2014, *95*, 391-399.
40. Gandolfo, A.; Bartolomei, V.; Gómez Alvarez, E.; Tlili, S.; Gligorovski, S.; Kleffmann, J.; Wortham, H. The effectiveness of indoor photocatalytic paints on NOx and HONO levels. *Appl. Catal. B: Environ.*, 2015, 84-90.
41. Gandolfo, A.; Rouyer, L.; Wortham, H.; Gligorovski, S. The influence of wall temperature on NO_2 removal and HONO levels released by indoor photocatalytic paints. *Appl. Catal. B: Environ.,* 2017, *209*, 429-436.
42. Liu, J.; Deng, H.; Lakey, P.S.J.; Jiang, H.; Mekic, M.; Wang, X.; Shiraiwa, M.; Gligorovski, S. Unexpectedly High Indoor HONO Concentrations Associated with Photochemical NO2 Transformation on Glass Windows. *Environ. Sci. Technol.*, 2020, DOI: 10.1021/acs.est.0c05624.
43. Liu, J.; Deng, H.; Sheng, L.; Jiang, H.; Mekic, M.; Zhou, W.; Wang, Y.; Loisel, G.; Wang, X.; Gligorovski, S. Light-Enhanced Heterogeneous Conversion of NO_2 to HONO on Solid Films Consisting of Fluorene and Fluorene/Na_2SO_4: An Impact on Urban and Indoor Atmosphere. *Environ. Sci. Technol.*, 2020, *54*, 11079-11086.
44. Han, C.; Yang, W.; Wu, Q.; Yang, H.; Xue, X. Heterogeneous photochemical conversion of NO_2 to HONO on the humic acid surface under simulated sunlight. *Environ. Sci. Technol.*, 2016, *50*, 5017-5023.

45. Zhou, S.; Young, C. J.; VandenBoer, T. C.; Kowal, S. F.; Kahan, T. F. Time-resolved measurements of nitric oxide, nitrogen dioxide, and nitrous acid in an occupied New York home. *Environ. Sci. Technol.*, 2018, *52(15)*, 8355-8364.
46. Brigante, M.; Cazoir, D.; D'Anna, B.; George, C.; Donaldson, D. J. Photoenhanced Uptake of NO_2 by Pyrene Solid Films. *J. Phys. Chem. A.*, 2008, *112*, 9503 -9508.
47. Yu, Z.; Liu, C.; Niu, H.; Wu, M.; Gao, W.; Zhou, Z.; Huang, Z.; Li, X. Real time analysis of trace volatile organic compounds in ambient air: a comparison between membrane inlet single photon ionization mass spectrometry and proton transfer reaction mass spectrometry. *Anal. Methods*, 2020, *12*, 4343–4350.
48. Liu, J.; Li, S.; Zeng, J.; Mekic, M.; Yu, Z.; Zhou, W.; Loisel, G.; Gandolfo, A.; Song, W.; Wang, X.; Zhou, Z.; Herrmann, H.; Li, X.; Gligorovski, S. Assessing indoor gas phase oxidation capacity through real-time measurements of HONO and NOx in Guangzhou, China. *Environ. Sci.: Processes Impacts*, 2019, *6*, 413-417.
49. Mekic, M.; Zeng, J.; Jiang, B.; Li, X.; Lazarou, Y. G.; Brigante, M.; Herrmann, H.; Gligorovski, S. Formation of toxic unsaturated multifunctional and organosulfur compounds from the photosensitized processing of fluorene and DMSO at the air-water interface. *J. Geophys. Res.: Atmos.*, 2020, *125*, e2019JD031839.
50. Mekic, M.; Wang, Y.; Loisel, G.; Vione, D.; Gligorovski, S. Ionic Strength Effect Alters the Heterogeneous Ozone Oxidation of Methoxyphenols in Going from Cloud Droplets to Aerosol Deliquescent Particles. *Environ. Sci. Technol.*, 2020, *54, 20*, 12898-12907.
51. Mekic, M.; Loisel, G.; Zhou, W.; Jiang, B.; Vione, D.; Gligorovski, S. Ionic-Strength Effects on the Reactive Uptake of Ozone on Aqueous Pyruvic Acid: Implications for Air–Sea Ozone Deposition. *Environ. Sci. Technol.*, 2018, *52*, 12306-12315.
52. National Renewable Energy Laboratory (NREL), American Society for Testing and Materials G-173-03 Reference Spectra, 2003.
53. Gandolfo, A.; Gligorovski, V.; Bartolomei, V.; Gomez Alvarez, E.; Tlili, S.; Wortham, H.; Kleffmann, J.; Gligorovski, S. Spectrally resolved actinic flux and photolysis frequency of key species within indoor environment, *Build. Environ*. 2016, *109*, 50–57.
54. Brauer, M.; Dumyahn, T. S.; Spengler, J. D.; Gutschmidt, K.; Heinrich, J.; Wichmann, H. E. Measurement of acidic aerosol species in eastern Europe: implications for air pollution epidemiology. *Environ. Health Perspect.*, 1995, *103(5)*, 482-488.
55. Rasmussen, T. R.; Brauer, M.; Kjaergaard, S. Effects of nitrous acid exposure on human mucous membranes. *Am. J. Respir. Crit. Care Med.*, 1995, *151*, 1504-1511.
56. Gómez Alvarez, E.; Amedro, D.; Afif, S.; Gligorovski, S.; Schoemacker, C.; Fittschen, C.; Doussin, J.F.; Wortham, H. Unexpectedly high indoor hydroxyl radical concentrations associated with nitrous acid. *Proc. Natl. Acad. Sci. U.S.A.*, 2013, *110(33)*, 13294-13299.
57. Lee, J. D.; Whalley, L. K.; Heard, D. E.; Stone, D.; Dunmore, R. E.; Hamilton, J. F.; Young, D. E.; Allan, J. D.; Laufs, S., Kleffmann, J. Detailed budget analysis of HONO in central London reveals a missing daytime source. *Atmos. Chem. Phys.*, 2016, *16*, 2747-2764.
58. Shi, X. W.; Ge, Y. F.; Zheng, J.; Ma, Y.; Ren, X. R.; Zhang, Y. C. Budget of nitrous acid and its impacts on atmospheric oxidative capacity at an urban site in the central Yangtze River Delta region of China, *Atmos. Environ.*, 2020, *238*, 117725.
59. Liu, J. Y.; Liu, Z. R.; Ma, Z. Q.; Yang, S. H.; Yao, D.; Zhao, S. M.; Hu, B.; Tang, G. Q.; Sun, J.; Cheng, M. T.; Xu, Z. J.; Wang, Y. S. Detailed budget analysis of HONO in

Beijing, China: Implication on atmosphere oxidation capacity in polluted megacity. *Atmos. Environ.*, 2020, *244*, 117957.
60. Nissenson, P.; Dabdub, D.; Das, R.; Maurino, V.; Minero, C.; Vione, D. Evidence of the water-cage effect on the photolysis of NO_3^- and $FeOH^{2+}$. Implications of this effect and of H_2O_2 surface accumulation on photochemistry at the airewater interface of atmospheric droplets. *Atmos. Environ.*, 2010, *44*, 4859-4866.
61. Zhang, X.; Barraza, K.M.; Upton, K.T.; Beauchamp, J.L. Time resolved study of hydroxyl radical oxidation of oleic acid at the airwater interface. *Chem. Phys. Lett.* 2017, *683*, 76–82
62. Freeman, J.L.B.; Baker, P. R. S.; Schopfer, F. J.; Woodcock, S. R.; Napolitano, A. d'Ischia, M. Nitro-fatty Acid Formation and Signaling. *J. Biol. Chem.*, 2008, *283*, 15515-15519.
63. Jain, K.; Sidda, A.; Marathi, A.; Roy,U.; Falck, J.R.; Balazy, M. The mechanism of oleic acid nitration by NO_2. *Free Radic. Biol. Med.*, 2008, *45*, 269-283.
64. Huie, R. E. The reaction kinetics of NO_2. *Toxicology*, 1994, *89*, 193-216.
65. Pryor, W. A.; Lightsey, J. W.; Church, D. F. Reaction of Nitrogen Dioxide with Alkenes and Polyunsaturated Fatty Acids: Addition and Hydrogen Abstraction Mechanisms. *J. Am. Chem. Soc.*, 1982, *104*, 6685-6692.
66. Bedini, A.; Maurino, V.; Minero, C.; Vione, D. Theoretical and experimental evidence of the photonitration pathway of phenol and 4-chlorophenol: A mechanistic study of environmental significance. *Photochem. Photobiol. Sci.*, 2012, *11*, 418-424.
67. Minero, C.; Maurino, V.; Bono, F.; Pelizzetti, E.; Marinoni, A.; Mailhot, G.; Carlotti, M. E.; Vione, D. Effect of selected organic and inorganic snow and cloud components on the photochemical generation of nitrite by nitrate irradiation, *Chemosphere,* 2007, *68*, 2111-2117.
68. Guan, C.; Li, X.; Zhang, W.; Huang, Z. Identification of Nitration Products during Heterogeneous Reaction of NO2 on Soot in the Dark and under Simulated Sunlight, *J. Phys. Chem. A.*, 2017, *121*, 482-492.
69. Bejan, I.; Abd El Aal, Y.; Barnes, I.; Benter, T.; Bohn, B.; Wiesen, P.; Kleffmann, J. The photolysis of ortho-nitrophenols: a new gas phase source of HONO, *Phys. Chem. Chem. Phys.,* 2006, *8*, 2028-2035.
70. Lee, J. D.; Whalley, L. K.; Heard, D. E.; Stone, D.; Dunmore, R. E.; Hamilton, J. F.; Young, D. E.; Allan, J. D.; Laufs, S.; Kleffmann, J. Detailed budget analysis of HONO in central London reveals a missing daytime source, *Atmos. Chem. Phys.*, 2016, *16*, 2747–2764.